ELSEVIER

Surface Science 492 (2001) 106–114

SURFACE SCIENCE

www.elsevier.com/locate/susc

Oxidation of ordered Pt–Sn surface alloys by O_2

Dmitri I. Jerdev, Bruce E. Koel *

Department of Chemistry, University of Southern California, Los Angeles, CA 90089-0482, USA

Received 16 October 2000; accepted for publication 12 June 2001

Abstract

We have studied the oxidation of two, ordered Pt–Sn surface alloys at 380–425 K using moderately high pressures of oxygen (O_2) at $Po_2 = 2 \times 10^{-2}$ Torr. Under these conditions, the surface oxygen concentration increased to a maximum oxygen uptake of $\Theta_O = 1.2$ ML (1 ML $= 1.505 \times 10^{15}$ atom/cm^2) for the (2×2)-Sn/Pt(1 1 1) alloy (with $\Theta_{Sn} = 0.25$) and $\Theta_O = 1.4$ ML for the $(\sqrt{3} \times \sqrt{3})R30°$-Sn/Pt(1 1 1) alloy (with $\Theta_{Sn} = 0.33$). Oxygen accumulation was accompanied by a shift in the Sn($3d_{5/2}$) XPS peak from 484.9 to 485.5 eV, with most of the pre-alloyed tin oxidized to a "quasi-metallic" state (a form more reduced than SnO). In addition, an oxidic state of Sn (with composition SnO or SnO_x, where $x < 2$) is formed. No change occurred in the Pt(4f) peaks, suggesting that no "Pt oxide" phase was formed under these conditions. On the (2×2)-Sn/Pt(1 1 1) alloy, oxygen uptake to $\Theta_O = 0.5$ ML was achieved instantly (in less than 10 s) and then occurred more slowly until a saturation uptake was reached. Two kinetic regions for oxygen uptake exceeding $\Theta_O = 0.5$ ML were distinguished, with apparent activation energies E_{app} of 14 and 20 kcal/mol for oxygen concentrations of $\Theta_O = 0.5$–0.8 and 0.8–1.0 ML, respectively. The oxygen uptake curve for the $(\sqrt{3} \times \sqrt{3})R30°$-Sn/Pt(1 1 1) alloy also displayed two distinct regions. In the first region, with $\Theta_O < 0.4$ ML, E_{app} was 9 kcal/mol. In the second region, with $\Theta_O \geqslant 0.4$ ML, oxidation proceeded with $E_{app} = 17$ kcal/mol. Overall, these results are consistent with previous studies on bulk Pt–Sn alloys, but new information is obtained on the role of alloy surface structure in controlling the initial stages of oxidation kinetics.

Keywords: Surface diffusion; Chemisorption; Thermal desorption; Isotopic exchange/traces

1. Introduction

Pt–Sn bimetallic catalysts are known for their performance in naphtha reforming and hydrogenation/dehydrogenation reactions of hydrocarbons. Addition of Sn to supported Pt catalysts decreases coke formation on the catalyst, enhances lifetime and increases selectivity. These phenomena have often been attributed directly to alloy formation and corresponding changes in the surface geometry [1,2] or increased mobility of adsorbed hydrogen [3].

Pt–Sn scatalysts have also been used in oxidation reactions, e.g., in low-temperature CO oxidation [4,5] and methanol electro-oxidation [6,7]. One exciting recent application is the selective partial oxidation of ethane (C_2H_6) to ethylene (C_2H_4) [8]. High selectivity (85%) was achieved by using very short (millisecond) contact times at high temperatures over a very heavily loaded Pt–Sn catalyst. Fundamental studies of the reaction of oxygen with model bimetallic Pt and Sn catalyst surfaces can

* Corresponding author. Tel.: +1-213-740-7036; fax: +1-213-740-2701.

E-mail address: koel@chem1.usc.edu (B.E. Koel).

0039-6028/01/$ - see front matter
PII: S0039-6028(01)01407-8

provide insight into surface changes of the catalyst induced by exposure to oxygen and by oxidation–reduction cycles used in catalyst regeneration [9,10]. Catalyst regeneration in many catalytic applications is a complicated process that leads to redispersion of active metal particles and changes the catalytic behavior depending upon the oxidation conditions or "history" of the catalyst [10].

Oxidation of bulk samples of polycrystalline and single-crystal Pt–Sn alloys has been interpreted as involving several forms of oxidized Sn. In addition to SnO and SnO_2, Hoflund and coworkers reported the formation of an intermetallic oxide with a Pt–O–Sn bond [11,12] in tin-oxide supported platinum samples and also a transitional oxide with a composition intermediate between SnO and SnO_2 [13]. However, careful oxidation kinetics studies using O_2 have not been done on well-defined, single crystal Pt–Sn alloys. Because the dissociative sticking coefficient of O_2 is small on Pt–Sn alloys, recent UHV studies have resorted to using more efficient oxidizing agents such as ozone (O_3) [14] or nitrogen dioxide (NO_2) [15] in order to probe aspects of this chemistry. Using O_3 as an oxidant, oxygen concentrations as high as $\Theta_O = 1.2$ ML were obtained at 300 K on Sn/Pt(1 1 1) alloys under UHV conditions. XPS showed that both Sn and Pt could be oxidized to oxidic forms using these oxidants.

Such UHV studies have been able to determine decomposition kinetics for these oxidized alloy surfaces. However, the Pt–O and Sn–O bond strengths are still not known because the activation energy of dissociative adsorption of O_2 on these surfaces is unknown. In this paper, we (i) determine activation energies for oxidation of the (2×2)- and $(\sqrt{3} \times \sqrt{3})R30°$-Sn/Pt(1 1 1) surface alloys at high pressures of O_2, and (ii) compare the chemical results of this oxidation procedure with that using more active oxidants such as O_3 and NO_2 under UHV conditions.

2. Experimental procedures

The experiments utilized a UHV surface-analysis chamber that was directly connected to a high-pressure reaction cell. The UHV chamber was equipped with a shielded, UTI-100C quadrupole mass spectrometer (QMS) for TPD studies, Φ 10-360 spherical capacitor analyzer (SCA) for Auger electron spectroscopy (AES), X-ray photoelectron spectroscopy (XPS) and low energy ion scattering spectroscopy (LEISS), Φ 15-120 4-grid low energy electron diffraction (LEED) optics, Φ 04-303 differentially-pumped ion gun, several multichannel-array gas dosers connected to precision leak valves, and several metal evaporators. XPS measurements were made by using a Φ 05-548 dual-anode X-ray source with a Mg anode ($MgK_\alpha = 1253.6$ eV). A Φ 04-015 electron gun was used for AES. The UHV chamber was pumped with a CTI Cryo-Plex 8 cryogenic pump (1500 l/s) and an ion pump (240 l/s) to provide a background pressure of 2×10^{-10} Torr.

The Pt sample was transferred between the analysis chamber and the high-pressure cell by means of a transfer rod passing through a differentially-pumped assembly of sliding seals. A gate valve separates the high-pressure cell from the UHV chamber when the reaction cell is pressurized. The reaction cell could be evacuated with a turbomolecular pump (Pfeiffer TMU 260) and it took only a few seconds to bring the cell from a pressure of 0.02 Torr O_2 to a pressure low enough to transfer the sample into the UHV chamber while maintaining a background pressure of 4×10^{-10} Torr.

The Pt(1 1 1) crystal had two polished sides oriented to the (1 1 1) crystal plane. The crystal was spot-welded between two tungsten wires (0.8-mm diameter) wrapped with Pt foil at the point of contact with the Pt crystal. The crystal could be resistively heated between 300 and 1200 K, as monitored by a chromel–alumel thermocouple that was spot-welded to the side of the crystal. Cleaning of the sample was performed in the UHV chamber by 1-keV Ar^+ ion sputtering, first with the sample held at 300 K for 5 min and then at 1000 K for 1 min. After this cleaning procedure, the sample was annealed at 1200 K for 30 s in UHV. The C(KLL) Auger peak, along with those for most common contaminants, was below the detection limit. Binding energies reported herein were obtained with the $Pt(4f_{7/2})$ peak set to 70.9 eV for the clean Pt(1 1 1) crystal.

The (2 × 2)-Sn/Pt(1 1 1) and ($\sqrt{3} \times \sqrt{3}$)*R*30°-Sn/Pt(1 1 1) surface alloys were both prepared using a procedure similar to that described by Paffet and Windham [16]. Sn was evaporated onto the Pt(1 1 1) surface at 300 K in UHV. This was followed by annealing the crystal to 1000 K for 10 s. The two surface alloys could be formed reliably, but LEED and XPS were used each time to insure proper alloy formation. Prior to all experiments, both alloys were characterized after preparation by a Sn($3d_{5/2}$):Pt($4f_{7/2}$) peak-height ratio in XPS of 0.35 for the (2 × 2) alloy and 0.41 for the ($\sqrt{3} \times \sqrt{3}$)*R*30° alloy. These alloys have been characterized previously by angle-dependent, LEISS [17], LEED I-V [18], and X-ray photoelectron diffraction (XPD) [19].

Oxidation of the ordered Sn/Pt(1 1 1) surface alloys was carried out in the reaction cell by using 0.02-Torr O_2. Research grade O_2 (Matheson, 99.999%) was used as supplied. Oxygen "uptake curves" were obtained by sequential, high-pressure O_2 exposures in the high-pressure cell and measurements of the intermittent oxygen concentration by using the O(1s) peak in XPS after the sample was transferred to the UHV chamber. The O(1s) signal was correlated to oxygen coverage by using the O(1s) XPS peak from an adsorbed CO monolayer on Pt(1 1 1) at 300 K which has $\Theta_{CO} = 0.49$ ML [20]. The temperature of the crystal was controlled to be constant (±2 K) at all times during the experiments. The highest temperature used for measuring the kinetics at 425 K was 175 K below the leading edge (600 K) of the first peak in O_2 TPD from the fully oxidized alloy [14]. This means that no strongly bonded oxygen was desorbed in the UHV environment. The choice of temperatures at which the uptake curves were taken was limited by the small exposures required at high temperatures and by the length of time necessary to carry out oxidation at low temperatures. Control experiments were done by exposing the alloys to identical oxygen exposures achieved by either two sequential exposures or a single, one-time O_2 exposure. The measured difference in oxygen coverages was only about 5%, which is within experimental error for the coverage determinations. Herein, one monolayer (ML) is defined as the Pt(1 1 1) surface concentration of 1.505×10^{15} atom/cm^2.

3. Results and discussion

In order to calculate oxygen coverages by using XPS, we assumed that oxygen resides either at the surface or in the very near-surface region. The O(1s) XPS signal is then proportional to the amount of oxygen accumulated, independent of the oxygen concentration. This is a reasonable assumption based on our previous studies [14,15]. Also Hoflund et al. [21] reported that all oxygen indeed stays in the surface region in experiments on Pt_3Sn bulk alloys at temperatures below 250°C (523 K).

Oxidation of the (2 × 2)-Sn/Pt(1 1 1) alloy at a pressure of 20-mTorr O_2 proceeded according to the oxygen uptake curves shown in Fig. 1. The curves exhibited two distinct kinetic regions. In the first region, where the oxygen concentration Θ_O was less than 0.5 ML, there was a very high rate of oxygen uptake as shown in the inset. Experiments with the sample at 380–425 K showed that a concentration of $\Theta_O = 0.5$ ML was achieved in less then 10 s. We did not measure further the kinetics at values of $\Theta_O < 0.5$ ML in this rapid uptake region. In the second region, where $\Theta_O > 0.5$ ML, the oxygen concentration grew monotonically until a saturation value of $\Theta_O = 1.2$ ML was achieved.

For oxidation of the ($\sqrt{3} \times \sqrt{3}$)*R*30° alloy at a pressure of 20-mTorr O_2, the oxygen concentration also increased monotonically with O_2 exposure and saturated at $\Theta_O = 1.4$ ML, as shown in Fig. 2. Two regions of oxygen concentration with different rates of oxygen uptake were also observed for this alloy, with a transition near $\Theta_O = 0.4$ ML. The oxidation rate was higher for $\Theta_O < 0.4$ ML than that for higher oxygen concentrations, but still lower than that for the corresponding low oxygen-coverage region on the (2 × 2)-Sn/Pt(1 1 1) alloy.

We observed no significant influence of the temperature on the saturation oxygen concentration on either alloy over the range of 380–425 K. However, temperature strongly influenced the uptake kinetics because oxygen accumulation is an activated process. Apparent activation energies E_{app} for oxygen accumulation on each alloy were determined using uptake curves taken at substrate

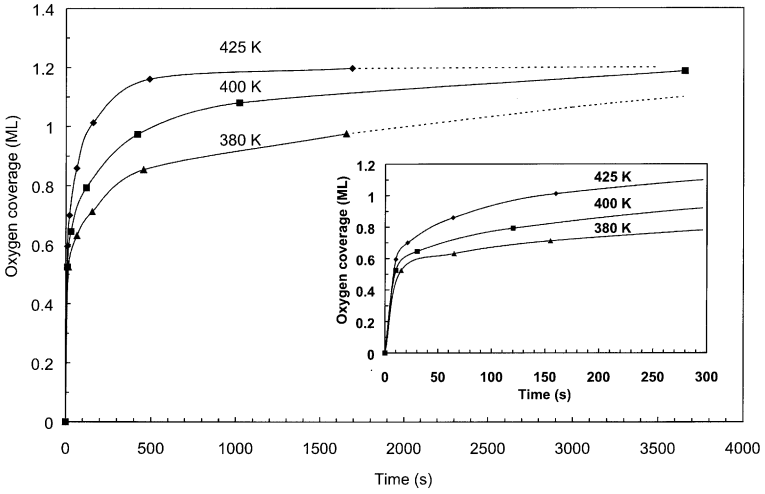

Fig. 1. Oxygen uptake from O_2 exposures on the (2×2)-Sn/Pt(1 1 1) alloy using $P(O_2) = 3 \times 10^{-2}$ Torr.

temperatures of 380, 400, and 425 K. Arrhenius plots (not shown) were constructed for several different regions of Θ_O, in order to allow for the possibility of Θ_O-dependent values of E_{app}. The results of this analysis are given in Table 1, where values for E_{app} are given only for those coverage regimes where significant differences were apparent. For the (2×2) alloy, we can only estimate an upper bound on the value of E_{app} at less than 7 kcal/mol by using the result that a coverage of $\Theta_O = 0.5$ ML was achieved in less than 10 s at 20-mTorr O_2 with the alloy at 380 K.

Oxygen uptake proceeds with a shift of the Sn(3d) XPS peaks to higher binding energy (BE) with increasing oxygen coverage on the both alloys. The clean, freshly prepared alloys were both characterized by a $Sn(3d_{5/2})$ peak at 484.9 eV BE. At the point where the maximal oxygen concentration was achieved, the $Sn(3d_{5/2})$ peak was obviously broadened by tin oxidation, as shown in Fig. 2. In order to determine the number of distinct chemical states of Sn, along with the relative concentrations of each, we decomposed the Sn(3d) XPS doublet by using curve-fitting. We made the following assumptions in performing this procedure: (i) the $Sn(3d_{5/2})$–$Sn(3d_{3/2})$ spin orbit splitting ($\Delta E = 8.42$ eV) and intensity ratio (3:2) were set to be the same for all three forms of Sn, independent of oxidation state; (ii) the peak full-width-at-half-maximum (FWHM) was set to a constant value of 1.1 eV for all forms of Sn; and (iii) the Sn(3d) peaks for the freshly prepared alloys, where Sn is in the metallic state, were used as the lineshape-template to fit all other Sn forms. The metallic Sn peaks were fit well by using a mixture of Lorentzian (70%) and Gaussian (30%) functions. Only the positions and intensities for each of the Sn forms were allowed to change during fitting. Fig. 3 compares measured data after background subtraction (shown as solid points) to the sum (solid curve) of the separate (dashed curves) peak contributions. Three tin peaks were found after the saturation oxygen concentration was reached on both alloys.

Table 1
Apparent activation energies E_{app} for oxidation of Sn/Pt(1 1 1) surface alloys at 380–425 K using $P_{O_2} = 0.02$ Torr

Alloy	Θ_O (ML)	E_{app} (kcal/mol)
(2×2)	0–0.5	<7
	0.5–0.75	14 ± 2
	0.75–1.0	20 ± 4
$(\sqrt{3} \times \sqrt{3})R30°$	0–0.4	9 ± 2.5
	0.4–1.3	17 ± 3

The assignments of the chemical origins of each of these peaks were made primarily on the basis of previous XPS studies of the oxidation of bulk, Pt_3Sn alloy single crystals [21,22]. First, the $Sn(3d_{5/2})$ component at 484.9 eV BE is from metallic, alloyed tin and accounted for ~5% of the

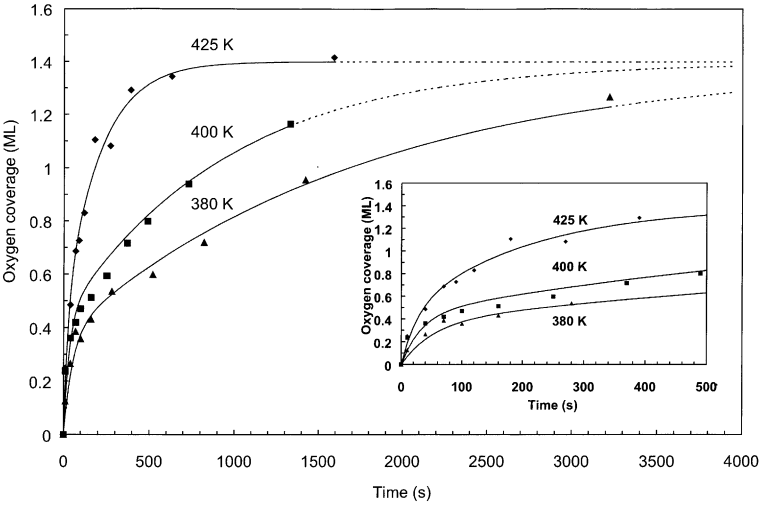

Fig. 2. Oxygen uptake from O_2 exposures on the $(\sqrt{3} \times \sqrt{3})R30°$-Sn/Pt(1 1 1) alloy using $P(O_2) = 3 \times 10^{-2}$ Torr.

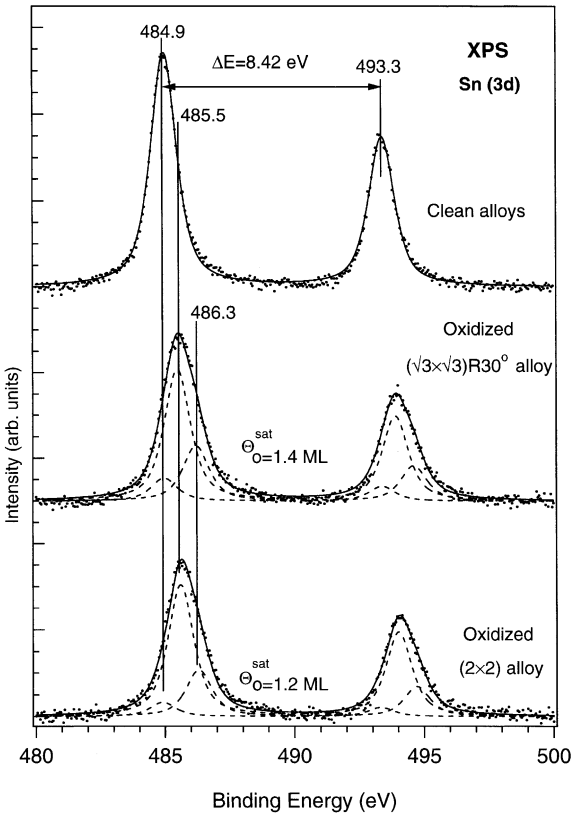

Fig. 3. Sn(3d) peaks in XPS for both the (2×2) and $(\sqrt{3} \times \sqrt{3})R30°$-Sn/Pt(1 1 1) alloys. The SCA was operated with a pass energy of 29 eV for an analyser resolution of 0.45 eV.

total Sn signal for both oxidized alloys in Fig. 3. Secondly, the peak at 485.5 eV BE is assigned to an oxidized form of Sn with a BE less than that for SnO and labeled as "quasimetallic" Sn by Rotermund and coworkers [23], and this accounted for 75% of the detected Sn. Thirdly, the peak at 486.3 eV can be assigned to "oxidic" Sn [11,12]. This component accounted for ~20% of the Sn signal. This peak may originate from SnO or SnO_2 phases, or both, because it has been reported to be difficult to clearly distinguish between them on the basis of the $Sn(3d_{5/2})$ BE [24]. However, observation of a $Sn(3d_{5/2})$ peak at 486.8 eV BE during O_3 oxidation studies of Sn/Pt(1 0 0) alloys [25], which is probably due to SnO_2, indicates that the peak at 486.3 eV should not be assigned to an SnO_2 phase. During the oxidation of Sn metal by O_2 [26] it was found that SnO, a transitional oxide that is possibly Sn_3O_4, and SnO_2 are all present, but SnO_2 was not formed in our experiments on these alloys. The above-cited intensities characterize the final values for uptake only, and they were different at lower values of Θ_O. As monitored by XPS (not shown), the amount of both "quasimetallic" and "oxidic" tin grew with increasing oxygen uptake, but the ratio of the amount of "quasimetallic" to "oxidic" tin decreased. Conversion of one form to the other could contribute to this change. The relative amounts of each Sn form was similar for

both alloys upon saturation of the oxidation treatment.

The accompanying O(1s) XPS spectra, after background subtraction, are shown in Fig. 4. The O(1s) peaks were decomposed into two components by fitting the data to the sum of two peaks with a Gaussian lineshape and FWHM = 1.1 eV. The peak at 529.7 eV BE is assigned to both quasimetallic and oxidic forms of tin. We assign the peak at 531.8 eV BE to contaminant hydroxyl (OH) species formed at high pressure due to a small amount of water contaminant. This peak accounted for only 13% of the O(1s) signal. The peak positions were identical and the intensity ratio of the two peaks were similar for both alloys. However, the amount of oxygen at saturation is slightly higher for the $(\sqrt{3} \times \sqrt{3})R30°$ alloy such that $\Theta_O = 1.4$ ML.

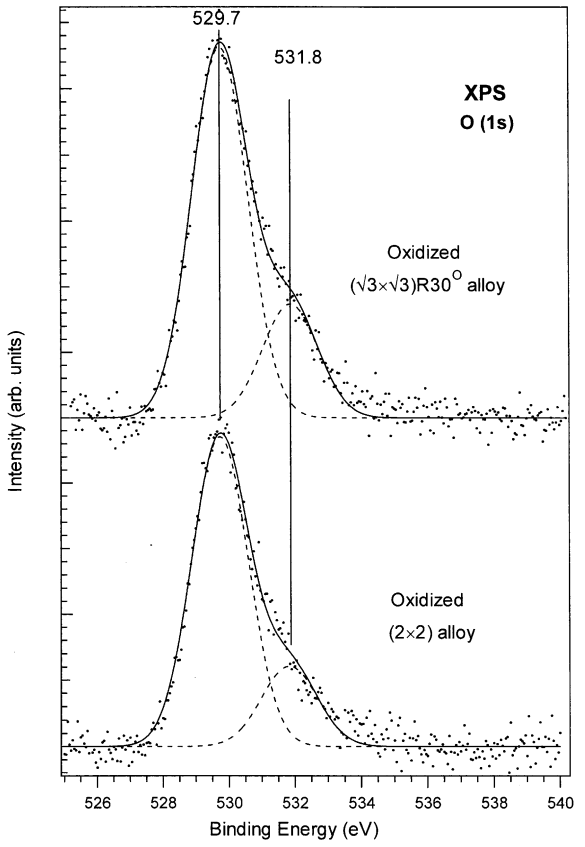

Fig. 4. O(1s) peaks in XPS for both the (2×2)- and $(\sqrt{3} \times \sqrt{3})R30°$-Sn/Pt(1 1 1) alloys at saturation oxygen coverage. The SCA was operated with a pass energy of 47 eV for an analyser resolution of 0.70 eV.

While there was a decrease in both of the $Pt(4f_{7/2})$ and $Sn(3d_{5/2})$ XPS peaks with increasing oxygen concentration, the $Pt(4f_{7/2})$:$Sn(3d_{5/2})$ peak area ratio did not change.

The Pt(4f) XPS peaks did not change position or width, and difference curves detected no specific features. Thus, no oxidation of Pt occurred under these conditions and the chemical state of Pt in these alloys was not affected by oxygen accumulation. This result is different from that when O_3 (ozone) was used as an oxidant on these Pt–Sn surface alloys at 300 K in UHV [14]. Ozone exposure formed an "oxidic" (PtO_x) phase. Ozone is a more powerful oxidant, even when used in UHV, than moderate pressures of oxygen. This is not surprising given that the O–O bond in O_3 is exceptionally weak (23 kcal/mol) compared to the 119-kcal/mol O–O bond in O_2. Consideration of the preequilibrium between the molecularly adsorbed precursor and chemisorbed oxygen adatoms leads to very high "effective" O_2 pressures when using O_3. Assuming no barrier for ozone dissociation, a barrier for dissociation of $O_{2(a)}$ of 12 kcal/mol and an adsorption energy for $O_{2)(a)}$ of 3 kcal/mol results in an enhancement factor of 10^8.

LEED showed a diffuse (1×1) hexagonal pattern when a saturation oxygen coverage was reached. Sn atoms are randomly displaced from their original positions to form the oxidized phases with increasing oxygen concentration. This results in the disappearance of the characteristic symmetry of the alloy surfaces. The oxygen-induced reconstruction of the surface, involving extraction of alloyed Sn atoms to form an overlayer with Sn–O bonding, has also been indicated in oxidation studies of these alloys in UHV using O_3 [14] and NO_2 [15].

The oxidation mechanism for these two Sn/Pt(1 1 1) surface alloys may be similar to that proposed by Rotermund et al. [23] for a Pd_3Sn bulk-terminated alloy. They considered that O_2 first dissociatively adsorbs on Pd clusters of some minimal size and then oxygen adatoms diffuse to Sn sites. They reported that the oxygen sticking coefficient dramatically decreased after a coverage of 0.3 ML was reached because each Sn atom is

associated with at least one O atom at that coverage. This mechanism is quite plausible for our Pt–Sn alloys, especially for the (2 × 2)-Sn/Pt(1 1 1) surface alloy because it is structurally the same as the (1 1 1) face of the Pd_3Sn bulk alloy. It seems likely that such a mechanism would also be the same for the $(\sqrt{3} \times \sqrt{3})R30°$-Pt/Sn(1 1 1) alloy, although oxidation might proceed more slowly because this alloy does not contain pure-Pt, three fold sites which might be necessary to facilitate dissociative adsorption of O_2.

In Fig. 5, we show schematic drawings of the two Sn/Pt(1 1 1) alloys and the Pt(1 1 1) surface as an aid to understanding differences in the initial oxygen uptake kinetics and oxidation on the two surfaces. The transition state for dissociative adsorption of O_2 on Pt(1 1 1) has one oxygen atom at a threefold, fcc-hollow site and one oxygen atom on top of an adjacent Pt atom [27] (Fig. 5A). Molecular dissociation occurs via movement of the oxygen atom at the atop site to one of the two available threefold, fcc-hollow sites (as indicated by the arrow in Fig. 5A). Dioxygen dissociation does not happen across twofold bridge sites because this would result in oxygen adatoms occupying two adjacent threefold sites (which is energetically unfavorable). Dissociative O_2 adsorption onto the Pt(1 1 1) surface in UHV forms a stable (2 × 2) adlayer of oxygen adatoms in which each Pt atom is bonded to only one O adatom. Formation of this ordered adlayer requires sufficient thermal energy to reach the equilibrium (2 × 2) configuration because both O atoms from O_2 dissociation initially reside within one unit cell (Fig. 5A). This is an important process that moves the adatoms further apart to occupy threefold, fcc-hollow sites where they have minimum energy. An activation energy for diffusion E_{diff} of oxygen adatoms in a (2 × 2) adlayer on Pt(1 1 1) has been estimated to be at least 22 kcal/mol [28], and at high oxygen concentrations this process could become rate-limiting for the dissociative adsorption of O_2.

We propose that initial O_2 dissociative adsorption on the (2 × 2)- Sn/Pt(1 1 1) alloy occurs similar to that on Pt(1 1 1) because both those surfaces have pure-Pt, threefold sites. Differences in the overall adsorption process could arise because of a stronger Sn–O bond compared to the Pt–O bond. Strong Sn–O bonding could make oxygen diffusion slower than that on the Pt(1 1 1) surface. If so, then oxygen adatoms from O_2 dissociative adsorption would be accommodated into the same unit cell, i.e., two oxygen adatoms per unit cell or $\Theta_O = 0.5$ ML. In this case, or if the dissociative pathway changed to accommodate both oxygen adatoms into pure-Pt threefold sites, the change in this situation at higher oxygen concentrations explains the large increase in E_{app} for $\Theta_O > 0.5$ ML. Diffusion of oxygen adatoms to Sn sites, or dealloying of Sn into the adlayer, is required for oxygen adatoms to populate additional threefold sites in the unit cell, i.e., to reach $\Theta_O = 0.75$ ML. It is even more energetically difficult to reach oxygen

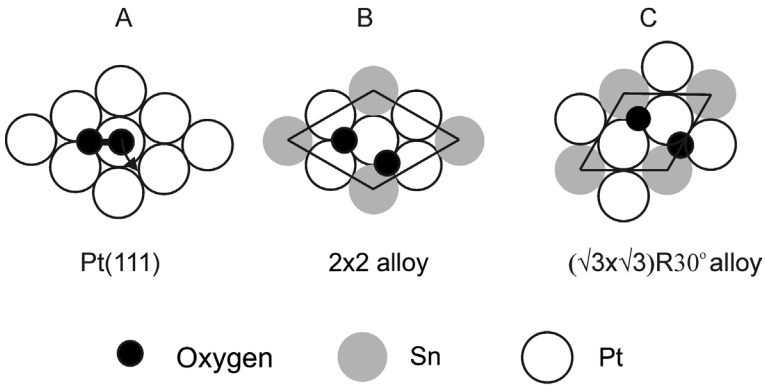

Fig. 5. Schematic, real-space model for discussion of dissociative oxygen adsorption on the (2 × 2)- and $(\sqrt{3} \times \sqrt{3})R30°$-Sn/Pt(1 1 1) alloys.

concentrations higher then 0.75 ML, because this requires bonding each surface Pt-atom to more than two oxygen adatoms. Thus, we would expect that another change in the kinetics, or in E_{app}, for $\Theta_O > 0.75$ ML. Our experimental data (Fig. 1) clearly show a change in the O_2 uptake rate at $\Theta_O = 0.5$ ML, which is in agreement with the proposed mechanism. The absence of a sharp feature in the O_2 uptake curves at $\Theta_O = 0.75$ ML could mean that E_{app} does not change strongly in that coverage region or that O-induced reconstruction of the alloy takes place at these coverages.

One would expect that the kinetics for initial O_2 uptake on the $(\sqrt{3} \times \sqrt{3})R30°$-Sn/Pt alloy would be different from those on Pt(1 1 1) and the (2×2)-Sn/Pt alloy, because there are no pure-Pt, threefold hollow sites on this surface. The process of dioxygen adsorption and dissociation must occur differently. There are two obvious possibilities: (a) dissociative adsorption on mixed Pt–Sn threefold sites, or (b) on defects. The latter implies a high rate of the oxygen adatom diffusion on the $(\sqrt{3} \times \sqrt{3})R30°$ alloy, which does not seem likely because of the high surface-tin concentration. Figs. 1 and 2 show that oxidation kinetics on this surface differ from those on the (2×2) alloy mostly in the region of the initial uptake. The rate was slower for the initial oxidation of the $(\sqrt{3} \times \sqrt{3})R30°$ alloy at $\Theta_O < 0.4$ ML. We attribute this to the smaller size of Pt ensembles that are available on this alloy surface, or more specifically, to the absence of all pure-Pt, threefold sites. In experiments probing the oxidation of polycrystalline tin by hyperthermal atomic oxygen beams, Hoflund and coworkers [24] concluded that O_2 dissociation was the rate-limiting step in the oxidation process. For these alloys, the presence of Pt ensembles that facilitate dissociative adsorption of oxygen would lead us to expect a higher initial oxygen uptake rate on the alloys compared to that of a pure Sn surface.

A schematic drawing of the $(\sqrt{3} \times \sqrt{3})R30°$ alloy in Fig. 5C shows how a similar O_2 dissociative mechanism and limited oxygen adatom diffusion would lead to a coverage of $\Theta_O = 0.5$ ML, with each Sn atom bonded to one oxygen adatom in a threefold site. The O_2 dissociative sticking coefficient should be reduced at higher coverages where each Sn atom has two oxygen nearest neighbors. This would result in two distinct kinetic regions on the oxygen uptake curves and a change of E_{app} at $\Theta_O = 0.5$ ML. We indeed observed two regions with different values for E_{app}, with a transition near $\Theta_O = 0.4$ ML. This is consistent with the proposed model, but it is unlikely that such a simple model can account for all processes occurring on the surface. The observed difference in saturation oxygen coverage (1.2 ML for the (2×2) alloy versus 1.4 ML for the $(\sqrt{3} \times \sqrt{3})R30°$ alloy) on the two alloys is probably simply related to the increased amount of Sn available for forming an oxidized Sn adlayer.

As a final point, we caution against the use of the E_{app} value given here to calculate Pt–O and Sn–O bond energies based on knowledge of the O_2 desorption activation energies reported previously [14]. Even though it is attractive to equate E_{app} with the activation energy for a dissociative O_2 adsorption elementary step, this needs to be established by additional measurements. More serious difficulty arises from the constraint of this approach on microscopic reversibility, i.e., to find D(Pt–O) or D(Sn–O) using E_{des} and E_{act}. It is doubtful that this can be satisfied in this type of experiment because oxygen adsorption is measured on well-defined, ordered alloy surfaces while oxygen desorption occurs from SnO nanoparticles on Pt–Sn alloy surfaces [29].

4. Conclusion

Oxidation kinetics was investigated for two, well-defined Sn–Pt surface alloys at 380–425 K in presence of 0.02-Torr O_2. Oxygen uptake curves monitoring oxygen accumulation for the (2×2)- and the $(\sqrt{3} \times \sqrt{3})R30°$-Sn/Pt(1 1 1) alloys differ greatly in the rate of initial uptake, but little in the oxygen saturation coverage. Fast oxygen uptake occurred until $\Theta_O \sim 0.5$ ML on both alloys and then slower uptake occurred to a saturation amount under these conditions of $\Theta_O = 1.2$ ML on the (2×2) alloy and $\Theta_O = 1.4$ ML on $(\sqrt{3} \times \sqrt{3})R30°$ alloy. The faster rate of initial oxygen accumulation on the (2×2) alloy indicates an

important role of the size of Pt ensembles, and perhaps specifically pure-Pt, threefold sites, in the dissociative adsorption of O_2. Oxygen accumulation proceeds on both alloys by oxidation of Sn in the alloy, forming throughout the process both "quasimetallic" (a form more reduced than SnO) and oxidic (SnO or SnO_x, where $x < 2$) forms. At saturation oxygen coverage, the surface contained 75% and 20% of these two forms, respectively. Oxidation of these Pt–Sn alloys resulted in disruption of the ordered alloy structure, but caused no change in the oxidation state of platinum. Apparent activation energies E_{app} for the oxidation process on the (2×2) alloy were <7 kcal/mol for $\Theta_O < 0.5$, 14 kcal/mol for $\Theta_O = 0.6$–0.8 ML, and 20 kcal/mol for $\Theta_O = 0.8$–1.0 ML. Values for E_{app} for the $(\sqrt{3} \times \sqrt{3})R30°$ alloy were 9 and 17 kcal/mol for $\Theta_O < 0.4$ ML and $\Theta_O > 0.4$ ML, respectively.

Acknowledgements

This work was supported by the Division of Chemical Sciences, Office of Basic Energy Sciences, US Department of Energy.

References

[1] R. Burch, J. Catal. 71 (1981) 348.
[2] L.K. Lok, N.A. Gaidaiand, S.L. Kiperman, in: M.J. Phillips, M. Ternan (Eds.), Proceedings, Ninth International Congress on Catalysis, Calgary, 1988, vol. 3, Chem. Inst. Canada, Ottawa, 1988, p. 1261.
[3] A. Sachdev, J. Schwankin, in: M.J. Phillips, M. Ternan (Eds.), Proceedings, Ninth International Congress on Catalysis, Calgary, 1988, vol. 3, Chem. Inst. Canada, Ottawa, 1988, p. 1275.
[4] D. Stark, A.P.H. Cross, G.J. Stewart, J. Phys. E: Sci. Instrum. 16 (1983) 158.
[5] G.B. Hoflund, B.T. Upchurch, E.J. Kielin, D.R. Schryer, Catal. Lett. 31 (1995) 133.
[6] K.J. Cathro, J. Electrochem. Soc. 116 (1969) 1608.
[7] M.M.P. Janssen, J. Moolhusyen, Electrochem. Acta 21 (1976) 861.
[8] A.S. Bodke, D.A. Olschki, L.D. Schmidt, E. Ranzi, Science 285 (1999) 712.
[9] J.P. Candy, F. Humblot, B. Didillon, F. Lepeltier, J.N. Basset, Stud. Surf. Sci. Catal. 126 (1999) 327.
[10] E. Lamypitara, L. Elouazzanibenhima, J. Barbier, M. Cahoreau, H. Caisso, J. Appl. Catal. 81 (1992) 147.
[11] D.F. Cox, G.B. Hoflund, H.A. Laitinen, Langmuir 1 (1985) 269.
[12] D.A. Asbury, G.B. Hoflund, Surf. Interface Anal. 9 (1986) 169.
[13] D.F. Cox, G.B. Hoflund, Surf. Sci. 151 (1985) 202.
[14] N.A. Saliba, Y. Tsai, B.E. Koel, J. Phys. Chem. B 103 (1999) 1532.
[15] D.H. Parker, B.E. Bartram, B.E. Koel, Surf. Sci. 217 (1989) 489.
[16] M.T. Paffet, R.G. Windham, Surf. Sci. 208 (1989) 34.
[17] S.H. Overbury, D.R. Mullins, M.T. Paffet, B.E. Koel, Surf. Sci. 254 (1991) 45.
[18] A. Atrei, U. Bardi, G. Rovida, M. Torrini, E. Zamazzi, P.N. Ross, Phys. Rev. 46 (1992) 1649.
[19] M. Galleotti, A. Atrei, U. Bardi, G. Rovida, M. Torrini, Surf. Sci. 313 (1994) 349.
[20] P.R. Norton, J.A. Davies, T.E. Jackman, Surf. Sci. 122 (1982) L593.
[21] D.A. Asbury, G.B. Hoflund, Surf. Sci. 199 (1988) 552.
[22] W. Unger, D. Marton, Surf. Sci. 218 (1989) L467.
[23] H.H. Rotermund, V. Penka, L.A. DeLouise, C.R. Brundle, J. Vac. Sci. Tech. 5 (4) (1987) 1132.
[24] J.F. Weaver, T.J. Campbell, G.B. Hoflund, G.N. Salaita, J. Electron. Spectrosc. Rel. Phenom. 106 (2000) 81.
[25] N.A. Saliba, C. Baur, D.E. Beck, B.E. Koel, in preparation.
[26] G.B. Hoflund, G.R. Corallo, Phys. Rev. B 46 (1992) 7110.
[27] A. Eiler, J. Hafner, Phys. Rev. Lett. 79 (1997) 22.
[28] V.P. Zhdanov, B. Kasemo, J. Catal. 170 (1997) 377.
[29] M.M. Batzill, D.E. Beck, B.E. Koel, App. Phys. Lett., submitted for publication.